



HAL
open science

**“Heavy-atom effects” in the parent
[1]benzochalcogenopheno[3,2-b][1]benzochalcogenophene
system**

Chengyuan Wang, Mamatimin Abbas, Guillaume Wantz, Kohsuke Kawabata,
Kazuo Takimiya

► **To cite this version:**

Chengyuan Wang, Mamatimin Abbas, Guillaume Wantz, Kohsuke Kawabata, Kazuo Takimiya.
“Heavy-atom effects” in the parent [1]benzochalcogenopheno[3,2-b][1]benzochalcogenophene system.
Journal of Materials Chemistry C, 2020, 8 (43), pp.15119-15127. 10.1039/d0tc01408g . hal-03000669

HAL Id: hal-03000669

<https://hal.science/hal-03000669>

Submitted on 19 Nov 2020

HAL is a multi-disciplinary open access archive for the deposit and dissemination of scientific research documents, whether they are published or not. The documents may come from teaching and research institutions in France or abroad, or from public or private research centers.

L'archive ouverte pluridisciplinaire **HAL**, est destinée au dépôt et à la diffusion de documents scientifiques de niveau recherche, publiés ou non, émanant des établissements d'enseignement et de recherche français ou étrangers, des laboratoires publics ou privés.

ARTICLE

“Heavy-atom Effects” in the Parent [1]Benzochalcogenopheno[3,2-*b*][1]benzochalcogenophene System

Received 00th January 20xx,
Accepted 00th January 20xx

Chengyuan Wang,^a Mamatimin Abbas,^b Guillaume Wantz,^b Kohsuke Kawabata,^{a,c} Kazuo Takimiya^{□,a,c}

DOI: 10.1039/x0xx00000x

[1]Benzochalcogenopheno[3,2-*b*][1]benzochalcogenophenes (BXXBs) have been the key π -conjugated core structures in the development of superior organic semiconductors for organic field-effect transistors (OFETs). The semiconducting properties of parent BXXBs, however, have not been well examined. In this work, we focus on the parent system and investigate the effect of different chalcogen atoms, i.e., sulphur, selenium or tellurium atoms, in the BXXB core on molecular electronic properties, crystal structures, intermolecular interaction, solid-state electronic structures, and carrier transport properties. Replacing sulphur atoms in [1]benzothieno[3,2-*b*][1]benzothiophene (BTBT) with selenium atoms marginally changes the molecular properties and their intermolecular interactions, thus resulting in similar herringbone packing structures in the solid state. The carrier mobilities of single-crystal (SC)-OFETs are higher for [1]benzoselenopheno[3,2-*b*][1]benzoselenophene (BSBS) than those for BTBT, which can be understood by the increase in the intermolecular electronic coupling in BSBS, originating in the larger atomic radius and more diffused electron cloud of selenium atoms than those of sulphur atoms. On the other hand, the packing structure of [1]benzotelluropheno[3,2-*b*][1]benzotellurophene (BTeBTe) is determined to be a dimeric herringbone structure. The crystal structure of BTeBTe being strikingly different from those of BTBT and BSBS can be explained by drastic change in the intermolecular interaction in the solid state. Furthermore, the BTeBTe-based SC-OFETs do not show transistor response. To elucidate these unexpected results, various experimental and theoretical approaches, e.g., evaluation of ionization potentials, band calculations, are examined. Through these approaches, a comprehensive view of the parent BXXB system is given, and also both the pros and cons of incorporation of heavy chalcogen atoms, positive and negative “heavy-atom effects”, in developing organic semiconductors are discussed.

Introduction

Large acenes and heteroacenes have been widely utilized as the active semiconducting material in organic field-effect transistors (OFETs) in the past decades.^{1,2,3} Thienoacenes that combines the structural features of acenes and thiophenes have been an important family of heteroacenes exhibiting promising carrier transport properties.^{4,5} [1]Benzochalcogenopheno[3,2-*b*][1]benzochalcogenophenes (BXXBs, Fig. 1) are among the most important and frequently used π -core structures for the development of superior organic semiconductors.⁶ In particular, the sulphur analogue, [1]benzothieno[3,2-*b*][1]benzothiophene (BTBT, Fig. 1), has afforded air-stable, high-performance organic semiconductors, e.g., symmetric^{7,8} and asymmetric derivatives⁹ with various substituents such as phenyl or alkyl groups at the 2,7-positions,¹⁰ or aromatic-fused derivatives^{11,12} acting as

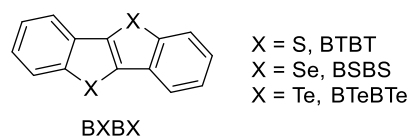


Fig. 1 Molecular structures of the parent BXXBs.

excellent active materials in OFETs via vapour- or solution-processes. A remarkable example is 2,7-dioctyl-BTBT (C₈-BTBT), which was reported to give the highest hole mobilities in OFETs with solution-deposited thin films.^{13,14}

In contrast to these fruitful results on the BXXB derivatives as organic semiconductors, the parent system, unsubstituted BXXBs, have been rarely examined as the active materials in OFETs.¹⁵ This initially prompted us to evaluate the semiconducting properties of the parent BXXB molecules. Furthermore, as the BXXB core has two chalcogenophene rings out of four aromatic rings, the parent system would be an ideal platform to elucidate so-called “heavy-atom effects”, the effects on the structure and properties that are caused by replacing the sulphur atoms in BTBT with selenium or tellurium atoms. The heavy atoms are believed to improve the semiconducting properties of the thienoacenes, owing to their large atomic radius, high polarizability, and diffused electron clouds, which are assumed to bring more efficient

^a Emergent Molecular Function Research Team, RIKEN Center for Emergent Matter Science (CEMS), 2-1 Hirosawa, Wako, Saitama 351-0198, Japan. E-mail: takimiya@riken.jp

^b Univ. Bordeaux, IMS, CNRS, UMR-5218, Bordeaux INP, ENSCBP, 33405 Talence, France.

^c Department of Chemistry, Graduate School of Science, Tohoku University, 6-3 Aoba, Aramaki, Aoba-ku, Sendai, Miyagi 980-8578, Japan.

† Electronic Supplementary Information (ESI) available: CCDC 1908813. For ESI and crystallographic data in CIF or other electronic format. See DOI: 10.1039/x0xx00000x

intermolecular electronic coupling in the solid state.^{16, 17, 18, 19} In fact, several approaches to take advantage of the heavy-atom effects in BXB derivatives have been examined.^{20, 21, 22} However, the existence of substituents, e.g., alkyl groups, makes it difficult to clarify the effects caused by the selenium atoms incorporated.

With these interests, we carried out systematic studies on parent BXBs with sulphur, selenium, and tellurium atoms (Fig. 1), in terms of molecular electronic properties, packing structures in the solid state, intermolecular electronic coupling, and carrier transport properties of single-crystal OFETs (SC-OFETs).

Experimental

Synthesis of materials

Parent BTBT,²³ BSBS,²¹ and BTeBTe²⁴ were synthesized based on the reported procedures. The materials were purified by multiple train-sublimation before device fabrication.

Device fabrication and characterization

The single crystals of the BXBs were grown by a physical vapour transport (PVT) method with argon as the carrier gas.²⁵ The SC-OFETs were fabricated in a bottom-gate top-contact (BGTC) device configuration with SiO₂ as the dielectric layer, or a top-gate top-contact (TGTC) device configuration with Parylene C as the dielectric layer, respectively (Fig. S1). To fabricate the BGTC SC-OFETs, free-standing single-crystals were laminated on an octadecyltrichlorosilane (ODTS)-modified, heavily doped n⁺-Si (100) wafer with 200 nm thermally grown SiO₂ ($C_i = 17.3 \text{ nF cm}^{-2}$). On top of the single crystals, colloidal graphite suspended in water was painted as source and drain electrodes.²⁶ To fabricate the TGTC SC-OFETs, ~500 nm Parylene C films ($\epsilon = 3.15$, C_i was calculated based on the exact thickness of Parylene C film, which was ~5 nF cm⁻²) was deposited on the single crystals with the source and drain electrodes on the substrate by a chemical vapour deposition (CVD) technique. On top of the Parylene C films colloidal graphite was painted as the gate electrode. The channel length and width of the SC-OFETs were optically determined under microscope. The devices were characterized at room temperature under ambient conditions with a Keithley 4200 semiconducting parameter analyser. Field-effect mobility (μ) was calculated in the saturation regime using the following equation (1):

$$I_D = C_i \mu (W/2L)(V_G - V_{th})^2 \quad (1)$$

where C_i is the total capacitance of the SiO₂ modified with ODTS or the Parylene C film. V_G and V_{th} are the gate and threshold voltages, respectively.

Theoretical calculations

The geometries of isolated molecules in the neutral and cationic states were optimized using the (U)B3LYP/3-21g or (U)B3LYP/6-31g(d) level with Gaussian 16 program package.²⁷ Note that the 6-31g(d) basis set does not cover tellurium atom, and thus the 3-21g basis set was used for the calculations. For BTBT and BSBS, calculations at the (U)B3LYP/6-31g(d) level of theory were

also carried out. The results were almost identical with those obtained with (U)B3LYP/3-21g (Fig. S2 and S3). The reorganization energy (λ) of the molecules was calculated by using the adiabatic potential energy surface method in equation (2):

$$\lambda = \lambda_0 + \lambda_+ = (E_0^* - E_0) + (E_+^* - E_+) \quad (2)$$

where E_0^* , E_0 , E_+^* , E_+ , represent the energies of a neutral molecule in the cationic geometry, a neutral molecule in the optimized geometry, a cationic molecule in the neutral geometry, and a cationic molecule in the optimized geometry, respectively.²⁸

Intermolecular electronic coupling (transfer integral, t) in different molecular dimers extracted from the single-crystal structures were calculated with the Amsterdam Density Functional (ADF) program.²⁹ With λ s and t s, anisotropic theoretical mobilities were calculated according to the reported procedure as described in Supporting Information (SI).^{30, 31}

Hirshfeld surfaces were computed on CrystalExplore 17.5 program to visualize intermolecular contacts in the crystalline state.^{32, 33} Intermolecular interaction energies for dimers of BTBT and BSBS extracted from the crystal structures were calculated by symmetry-adapted perturbation theory (SAPT) calculations with jun-cc-pvdz level using the PSI4 program package.^{34, 35} Band structure calculations were carried out with Crystal17 program at the B3LYP/3-21g level of theory using $4 \times 4 \times 4$ k-point Pack-Monkhorst net with the geometry of BTBT, BSBS, and BTeBTe determined by the single crystal X-ray analysis.³⁶ The carrier effective masses were evaluated by parabolic-fitting at the band extrema (Γ -Y direction).³⁷

Results

Physicochemical properties of BXBs

Fig. 2a shows the UV-Vis absorption spectra of the BXBs in chloroform. BTBT and BSBS have similar absorption bands, the latter of which are slightly red-shifted; the on-set of absorption for BSBS is 356 nm, which corresponds to the optical bandgap (E_g) of 3.48 eV, whereas those for BTBT are 342 nm and 3.63 eV, respectively. In the cyclic voltammograms (CVs) in benzonitrile solution (Fig. 2b), BTBT and BSBS show one reversible or irreversible oxidation peak, respectively. The onsets of the oxidation peaks (E_{onset}^{OX}) of BTBT and BSBS are 0.93 and 0.80 V versus Fc⁺/Fc, respectively, which correspond to the HOMO energy levels of -5.73 and -5.60 eV, respectively. The similarities of BTBT and BSBS in the absorption spectra and CVs suggest that the substitution of sulphur with selenium atoms marginally influences the electronic structure of the molecules (Table 1).

In contrast, the absorption spectrum and CV of BTeBTe are remarkably different from those of BTBT and BSBS; the largely red-shifted absorption with the on-set of 396 nm ($E_g = 3.13 \text{ eV}$, Fig. 2a) and two irreversible oxidation peaks observed in CV, where the onset of the first oxidation peak is 0.44 V, corresponding to the HOMO level of -5.24 eV, which is markedly higher than those of BTBT and BSBS. Table 1 summarizes the energy levels and optical bandgaps of BXBs.

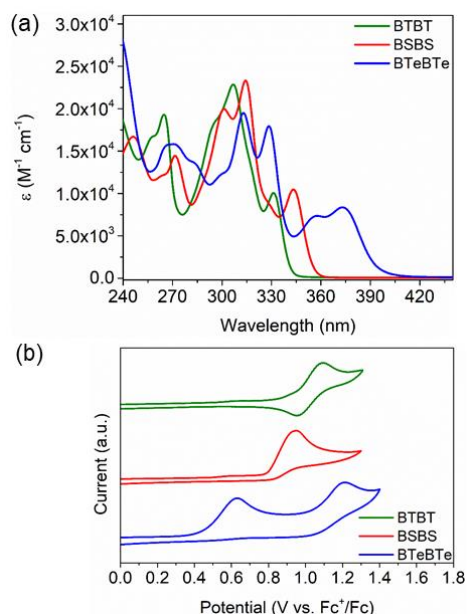


Fig. 2 (a) UV-vis absorption spectra in the chloroform solution and (b) cyclic voltammograms in the benzonitrile solution of BTBT, BSBS, and BTeBTe.

These empirical electronic properties can be qualitatively reproduced by the theoretical calculations (Fig. S2); for example, the HOMO energy levels are calculated to be -5.79 , -5.51 , and -5.37 eV for BTBT, BSBS, and BTeBTe, respectively. From the experimental results, it is obvious that the substitution of the selenium in BSBS with tellurium atoms yields more pronounced effects on the molecular electronic properties than the substitution of the sulphur in BTBT with selenium atom. In particular, the rise of HOMO energy level is remarkable for BTeBTe. This can be explained by the theoretical calculations; in the calculated distribution of HOMO coefficients of BTeBTe, contribution of the tellurium atoms is very large; the coefficients are localized on the tellurium atoms, implying that the nature of BTeBTe's HOMO is largely affected by the tellurium atoms (Fig. 3). This is consistent with the lowest

Table 1. Summarized energy levels and optical bandgaps of the BXBs

compound	$E_{\text{onset}}^{\text{ox}}/V$	HOMO ^b / eV	LUMO ^c / eV	E_g^d / eV
BTBT	0.93	-5.73	-2.10	3.63
BSBS	0.80	-5.60	-2.12	3.48
BTeBTe	0.44	-5.24	-2.11	3.13

^a Versus Fc/Fc⁺. ^b Determined from the equation; HOMO = $-4.80 - E_{\text{onset}}^{\text{ox}}$. ^c Determined from the equation; LUMO = HOMO + E_g . ^d Determined from the equation; $E_g = 1240/(\text{onset of absorption})$.

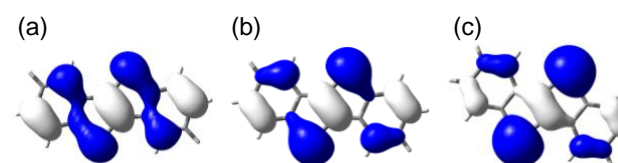


Fig. 3 The HOMO of (a) BTBT, (b) BSBS and (c) BTeBTe calculated at B3LYP/3-21g level.

aromatic stabilization of tellurophene among three chalcogenophenes (thiophene, selenophene and tellurophene);³⁸ the aromatic character of tellurophene ring in BTeBTe could marginally contribute to a total stabilization in the four fused-aromatic system, which is contrasted to the corresponding thiophene and selenophene ring in the BTBT and BSBS framework (Fig. S9).

Packing structures in single crystals

The single-crystal structures of BTBT^{6, 39} and BSBS²⁰ have been already reported. As shown in Fig. 4a and 4b, BTBT and BSBS are of isostructure with a typical herringbone packing with a monoclinic $P2_1/c$ space group. The distances between the centroids in the edge-to-face and edge-to-edge dimers are 5.01 and 5.89 Å in BTBT and 5.18 and 6.03 Å in BSBS, respectively. The dihedral angles between the edge-to-face dimers are 58.08° for BTBT and 62.09° for BSBS, respectively. These marginal differences in the single-crystal structures of BTBT and BSBS suggest that the substitution of the sulphur with selenium

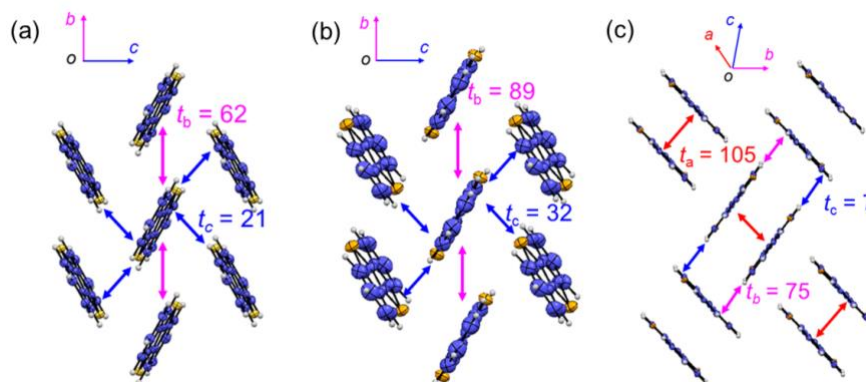


Fig. 4 Packing structures and intermolecular electronic couplings in the crystals of (a) BTBT, (b) BSBS, and (c) BTeBTe. The molecules are projected along the molecular long-axis direction. The non-hydrogen atoms are displayed in the ellipsoid plot with 50% probability.

atoms has minute influence to the molecular organization in the solid state.

In sharp contrast to the substitution of the sulphur with selenium atoms, the substitution with tellurium atoms drastically alters the packing structure. BTeBTe shows a dimeric herringbone packing with a monoclinic $P2_1/c$ space group (Fig. 4c). Within the dimer, the molecules are parallel with large displacement mainly along the molecular long-axis. Between the dimers, the molecules show slipped edge-to-face organization.

The fact that only the tellurium analogue, BTeBTe, crystallizes into different packing structure from those of the sulphur and selenium analogues (BTBT/BSBS) is contrasted from another chalcogenophene-containing system, benzo[1,2-*b*:4,5-*b'*]dichalcogenophenes, where all the sulphur, selenium, and tellurium analogues crystallize into the same herringbone packing.⁴⁰ Different trends in these systems imply that the position of the chalcogen atoms in the molecular backbone play an important role in defining the packing structure in the solid state (vide infra).

Single-crystal OFETs

One of practical reasons why the carrier transport properties of parent BXBs have never been reported is that uniform thin films of these materials can not be formed by the ordinary vacuum deposition. In our experiments, the vacuum deposition of BTBT and BSBS did not afford continuous thin films on the substrates. BTeBTe was successfully deposited on the substrates, but the thin films were almost amorphous and discontinuous, and accordingly not suitable as the active channel for OFETs (Fig. S5). Thus, SC-OFETs should be the choice for investigating carrier transport properties of BXBs. In addition, the SC-OFETs can minimize detrimental factors that hinder the carrier transport, i.e., grain boundaries, disordered

packing, and thus the devices well reveal the intrinsic electronic properties of materials.

The free-standing thin platelet crystals of BXBs were successfully obtained through the PVT technique. The single crystals laminated on the substrates were characterized by out-of-plane X-ray diffraction (XRD). The XRD patterns of the BXB single crystals on the substrate consist of only $h00$ peaks, judging from the powder patterns simulated from the single crystal data (Fig. S6), indicating that the crystallographic a -axes are in the out-of-plane direction. This corresponds to the end-on molecular orientation on the substrates, and the crystallographic bc plane is parallel to the substrate for all the BXB crystals (Fig. 4).

The carrier transport channels of the BXBs were determined based on the facet angles of the single crystals. In the BTBT and BSBS single crystals, the molecules with the edge-to-edge molecular organization, in other words, crystallographic b -axis, give the most efficient orbital overlaps (Fig. 4, see also Discussion section), and thus this direction was selected as the FET channel in the SC-OFETs. The BTBT and BSBS single crystals exhibited similar facet angles with 108° corresponds to the dihedral angle of 011 and 0-11 directions (Fig. S7). Thus, the bisector direction of this facet angle was determined to be the edge-to-edge direction. In the BTeBTe single crystals, the most efficient carrier transport direction should be along the orthogonally packed dimer molecules. The facet angle with 118° corresponds to the dihedral angle of 01-1 and 011 directions (Fig. S7). Therefore, the facet edge direction was selected as the channel in the BTeBTe-based SC-OFETs.

We noticed that thermal deposition of the gold source and drain electrodes on top of the crystals caused serious damages to the single crystals of BXBs due to a large amount of heat during the deposition process. Instead, colloidal graphite was

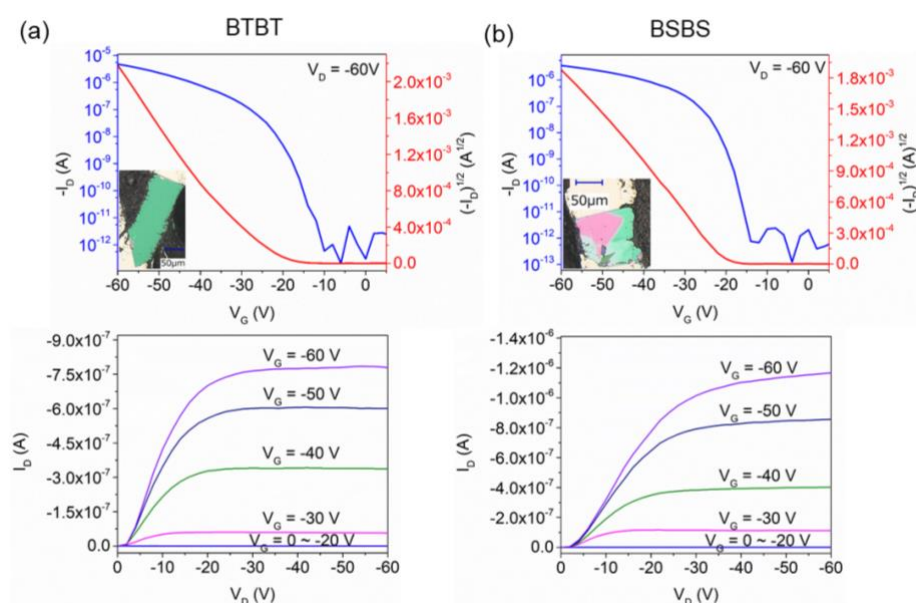


Fig. 5 Transfer (top) and output (bottom) curves of the BGTG-SC-OFETs based on (a) BTBT and (b) BSBS.

Table 2. Device characteristics of the BTBT/BSBS-based SC-OFETs

compound	mobility / $\text{cm}^2 \text{V}^{-1} \text{s}^{-1\text{a}}$	V_{th} / V	on/off ratio
BTBT	0.24 (0.36) ^b	-27.8 ^b	$10^6 - 10^{7\text{b}}$
	0.027 (0.041) ^c	-14.7 ^c	$10^4 - 10^{5\text{c}}$
BSBS	0.70 (0.90) ^b	-23.0 ^b	$10^6 - 10^{7\text{b}}$
	0.097 (0.13) ^c	-1.4 ^c	$10^4 - 10^{5\text{c}}$

^a The average mobilities are based on more than 10 devices, and values in parentheses are the highest mobilities. ^b BGTC SC-OFETs. ^c TGTC SC-OFETs.

painted as the source and drain electrodes, which turned out not to cause any damage to the single crystals.²⁶ The single crystals of BXBs prepared by the PVT method have a thickness of 300–500 nm. With such thin platelet single crystals, SC-OFETs with BGTC device configuration were fabricated (Fig. S1). As shown in Fig. 5, the BGTC SC-OFETs based on BTBT and BSBS exhibited typical transistor characteristics. The former showed mobilities of up to $0.36 \text{ cm}^2 \text{V}^{-1} \text{s}^{-1}$ (average: $0.24 \text{ cm}^2 \text{V}^{-1} \text{s}^{-1}$). The mobilities extracted from the BSBS based devices were up to $0.90 \text{ cm}^2 \text{V}^{-1} \text{s}^{-1}$, (average: $0.70 \text{ cm}^2 \text{V}^{-1} \text{s}^{-1}$), which is approximately 3 times higher than those of the BTBT-based ones. The devices with a BTeBTe single crystal did not show any transistor responses.

The TGTC SC-OFETs (Fig. S1) were also fabricated to examine the effect of device configurations on the device characteristics. As shown in Fig. S8, the TGTC SC-OFETs based on BTBT and BSBS exhibited typical transistor characteristics. The BTBT devices showed mobilities of up to $0.041 \text{ cm}^2 \text{V}^{-1} \text{s}^{-1}$ (average: $0.027 \text{ cm}^2 \text{V}^{-1} \text{s}^{-1}$), which are around one order of magnitude lower than those of the corresponding BGTC devices. Similarly, the mobilities of the BSBS devices were up to $0.13 \text{ cm}^2 \text{V}^{-1} \text{s}^{-1}$, (average: $0.097 \text{ cm}^2 \text{V}^{-1} \text{s}^{-1}$), which are about 8 times lower than those of the corresponding BGTC devices, but around 4 times higher than those of the BTBT-based TGTC devices. The BTeBTe-based devices again did not show any transistor responses. Table 2 summarizes the device characteristics of the SC-OFETs of BTBT and BSBS.

Evaluation of carrier transport properties of BXB single crystals with two different device configurations tells us several important information. First, the BGTC devices always afforded better device performances than those of TGTC ones. One of possible reasons for this is poor injection characteristics in TGTC devices (see the output characteristics in Fig. S8), which can affect the total device performances. The reasons for this injection issue are not clear, but we can conclude that the BGTC device configuration is more suitable to characterize the carrier transport properties of BTBT and BSBS. Second, although the mobilities obtained from the BTBT and BSBS devices are not comparable with ones from the state-of-the-art materials with largely π -extended systems, their performances are reasonably high for the small π -conjugated system with four fused aromatic rings. Third, regardless of the device configurations, BSBS single crystals always showed higher mobilities than that of BTBT (3 times high in BGTC SC-OFETs, 4 times in TGTC SC-OFETs,

respectively), clearly indicating that the carrier transport in BSBS is more efficient than that in BTBT. Finally, even with different device configurations, the single crystals of BTeBTe did not act as the transistor channel, implying that the BTeBTe crystals could not be intrinsically suitable for transistor applications (vide infra).

Discussion

Effect of chalcogen atoms on intermolecular contacts in the solid state: Hirshfeld surface analysis

As discussed already, the effect of chalcogen atoms in the BXB core on the packing structure is remarkable; in particular, the incorporation of tellurium atoms brings drastic change in the packing structure. This implies that the chalcogen atoms can alter the intermolecular contacts in the solid state. Hirshfeld surface analysis, an effective measure to visualize intermolecular contacts, was thus carried out. As shown in Fig. 6a, the Hirshfeld surface of BTBT mapped with d_e (distance from the surface to the nearest nucleus external to the surface) exhibits intermolecular contacts along the molecular edge and π -faces (large green and red regions on the surface). The ratio of these intermolecular contacts (i.e., C–H and S–C contacts) comprises more than 50% (Fig. S10) of the total intermolecular contacts, suggesting that the edge-to-face intermolecular interaction contributes to stabilize the herringbone packing of BTBT. This is further confirmed by the calculations of intermolecular interaction energies (Table S1) in the edge-to-face and edge-to-edge dimers by the SAPT method. The intermolecular interaction energy of edge-to-face dimer is $-11.24 \text{ kcal mol}^{-1}$, and this is approximately 1.4 times larger than that of edge-to-edge dimer ($-8.35 \text{ kcal mol}^{-1}$), in which the dispersion gives the largest contribution ($-15.03 \text{ kcal mol}^{-1}$ for the edge-to-face dimer and $-10.89 \text{ kcal mol}^{-1}$ for the edge-to-edge dimer, respectively).

From these analyses, the herringbone packing of BTBT is concluded to be a dispersion-driven packing structure that is facilitated by the edge-to-face CH- π contacts similar to the acenes and other thienoacenes.⁴¹ The Hirshfeld surface analysis as well as the SAPT calculations of BSBS are basically the same as those of BTBT,

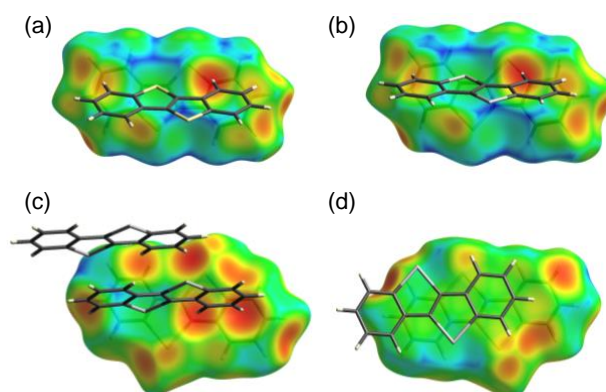


Fig. 6 Hirshfeld surface and ratio of intermolecular short contacts of the BXB molecules extracted from the respective crystal structures mapped with d_e , (a), BTBT, (b) BSBS, and (c and d) BTeBTe for the CH- π side and π - π side.

in terms of the distribution and ratio of each intermolecular contact and energetical stabilization (Fig. 6b and Fig. S10).

The Hirshfeld surface of BTeBTe is significantly different from those of BTBT and BSBS (Fig. 6c and 6d). Although a similar edge-to-face CH- π contacts between the hydrogen atoms in the benzene rings and the π -surface are observed, only the part of molecular edges are involved in the contacts. This is obviously owing to the existence of tellurium atoms in the middle of the molecule. In other words, because of the large atomic radius and elongated C-Te bonds, the tellurium atoms in the BTeBTe core protrude at the molecular edges, resulting in the whole molecular edges unavailable for the edge-to-face CH- π contacts that play the key role in the formation of herringbone packing structure. In addition, the incorporation of tellurium atoms makes the molecular shape rather "square-like" (Fig. 6c and 6d), which is contrasted to the rectangular-shaped BTBT and BSBS (Fig. 6a and 6b). As two-dimensional extension of π -conjugated systems often makes the π - π stacking structure favourable,^{42, 43} the co-facial dimer of BTeBTe can be rationally explained. Because of such characteristic molecular shape of BTeBTe, the ratio of C-H contact is decreased (Fig. S10), and instead the intermolecular contacts including the tellurium atoms, i.e., Te-H and Te-C, increase significantly; more than 30% for BTeBTe, whereas ca. 25 (26)% of S(Se)-H and S(Se)-C for BTBT (BSBS). We can thus conclude that the molecular shape of BTeBTe changes the intermolecular interaction and thereby the packing structure. This is, in turn, regarded as a significant "heavy-atom effect" caused by the tellurium atoms in the BXB core. In fact, substitution of one sulphur atom in BTBT with a tellurium atom, e.g., [1]benzotelluropheno[3,2-*b*][1]benzothiophene, has a similar dimeric herringbone packing to that of BTeBTe.⁴⁴

Effect of chalcogen atoms on intermolecular electronic coupling in the solid state and transport properties

BTBT and BSBS. BTBT shows typical anisotropic orbital overlaps with moderately large electronic coupling (t). The t along the edge-to-edge direction (crystallographic b -axis, t_b) is 62 meV, and that along the edge-to-face direction (t_a) is 21 meV (Fig. 4a). A similar anisotropic electronic coupling to that of BTBT is observed in BSBS. The t along the edge-to-edge (crystallographic b -axis, t_b : 89 meV) and edge-to-face (t_c : 32 meV) directions are about 1.5 times larger than the corresponding ones in BTBT. The remarkable increase of t s in BSBS could be regarded as a positive "heavy-atom effect", i.e., enhanced electronic couplings between neighbouring molecules thanks to the larger atomic radius and more diffused electron clouds of selenium than those of sulphur atoms. This is reasonably consistent with the higher mobilities of the BSBS-based SC-OFETs than that of the BTBT counterpart.

To get further insight into the carrier transport properties of parent BTBT and BSBS, their theoretical anisotropic mobilities under the ideal environment are simulated in the hopping regime by utilizing the Marcus/Hush model.^{30,45} As BTBT and BSBS form lamellar structures in the single crystals and adopt

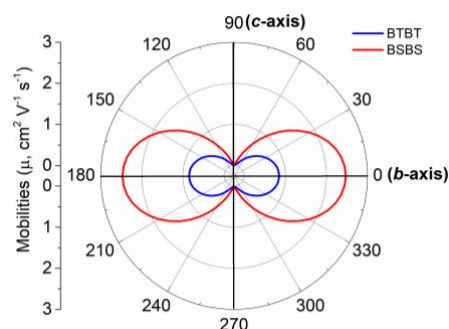


Fig. 7 Calculated anisotropic mobilities in the ideal BTBT and BSBS crystals (the 0° and 180° directions are along the edge-to-edge direction (crystallographic b -axis for BTBT and BSBS, see also Fig. S11).

the end-on molecular orientation on the substrate, the crystallographic bc plane should be considered as the conducting layer.³¹ Inside the conducting layer, the carrier transport can be determined by combining the electronic couplings from all the hopping pathways. The anisotropic mobilities were calculated with the b -axis direction as the reference axis (Fig. S11, see SI for details).

The key parameters dictating the carrier mobility in the hopping regime are t (Fig. 4) and reorganization energy (λ). The λ s of BTBT and BSBS are calculated to be 225 and 198 meV, respectively. The lower λ of BSBS than that of BTBT can be explained by the more diffused molecular orbitals of BSBS than that of BTBT thanks to the selenium atoms, which makes the radical cations of BSBS less deformed during the carrier transport. The theoretical mobilities of BTBT are calculated to be 0.01 (along c -axis) – 0.85 (along b -axis) $\text{cm}^2 \text{V}^{-1} \text{s}^{-1}$, and those of BSBS are in the range of 0.04 (along c -axis) – 2.47 (along b -axis) $\text{cm}^2 \text{V}^{-1} \text{s}^{-1}$ (Fig. 7). Since the difference in λ between BTBT and BSBS is not that large, the higher mobilities of BSBS are mainly attributed to the larger intermolecular electronic couplings than those of BTBT. The theoretical calculations indicate that the substitution of the sulphur with selenium atoms does improve the carrier transport properties mainly by enhancing the intermolecular electronic couplings. The increasing trend of the theoretical mobilities is well consistent with the empirical results (Table 2). On the other hand, the theoretical mobilities are approximately 3 times higher than the experimental values, implying that the SC-OFETs still have some room for improvement.

BTeBTe. The BTBT-BSBS system is regarded as an ideal case for the positive "heavy-atom effect" in organic semiconductors, where the heavy atom, i.e., selenium, does contribute to enhance intermolecular electronic coupling and thereby transport properties in the solid state. BTeBTe, on the other hand, is not on the same line as such an ideal case, because of the drastic change in the packing structure from the herringbone to dimeric herringbone packing (Fig. 4c). However, the change in the packing structure can not solely explain why the BTeBTe-based SC-OFET did not show any transistor

characteristics. To clarify this, we first look at the intermolecular electronic coupling in the crystal structure of BTeBTe.

As shown in Fig. 4c, the intermolecular electronic coupling within the BTeBTe dimers is as large as 105 meV (t_a). Since there is certain displacement along the long molecular axis in the dimers, the intermolecular electronic couplings between the molecules in the neighbouring dimers are inequivalent. The less displaced molecules in the neighbouring dimers yield fairly large t (t_b , 75 meV), and in contrast, t_c for the largely displaced molecule is only 7 meV. It seems that the large t in the dimer locally facilitates the carrier transport, but the overall transport is affected by the intermolecular electronic coupling in all the direction including the ones with very poor electronic coupling (t_c , 7 meV). In other words, this ineffective path might be the bottleneck of carrier transport in the bc conducting plane. However, this does not reasonably explain why the BTeBTe based SC-OFETs showed no transistor responses. In fact, a similar dimeric herringbone structure was reported for dinaphtho[1,2-*b*:1',2'-*f*]thieno[3,2-*b*]thiophene, the thin-film transistors of which show decent transistor characteristics with mobilities of up to $10^{-2} \text{ cm}^2 \text{ V}^{-1} \text{ s}^{-1}$.⁴⁶

In order to get further insight into BTeBTe, two additional analyses were carried out. One is to evaluate the ionization potential (IP) of the solid samples of BTeBTe (Fig. S12) by means of the photoelectron spectroscopy in air to confirm the efficiency of hole injection from the electrode into the SC-OFETs. IPs of BTBT, BSBS and BTeBTe were thus experimentally determined to be 5.8, 5.6 and 5.4 eV, which are mostly consistent with their HOMO energy levels electrochemically determined (Table 1). This means that the hole injection from the electrode should be better in the BTeBTe-based SC-OFETs

than those of BTBT- and BSBS-based ones, which can rule out the hole injection issue from the possible causes that make the BTeBTe-based SC-OFETs no response.

The other is to calculate the band structure of BTeBTe together with BTBT and BSBS, instead of the calculation of anisotropic mobilities, since the latter method is not applicable to BTeBTe with the dimeric herringbone structure owing to indeterminable hopping pathways. As depicted in Fig. 8 and Fig. S13, the calculated band structures of BTBT and BSBS have a similar dispersion, where the band width of Γ - Y direction, which corresponds to the crystallographic b -axis is larger than that of Γ - Z direction (crystallographic c -axis), being consist with the anisotropy of electronic couplings of HOMO (Fig. 4a and 4b). For BSBS, the band width in the Γ - Y direction is as large as 481 meV, which is approximately 1.6 time larger than that of BTBT (292 meV). In contrast, the band dispersion of BTeBTe is different from those of BTBT and BSBS reflected by the dimeric herringbone structure, and the largest band width of 243 meV is calculated for the Γ - Y direction. Although the smallest band width of BTeBTe among the three compounds is reasonable for the strong dimerization of molecules, it could not directly rationalize the silent behaviours of the BTeBTe-based SC-OFETs. Furthermore, effective carrier masses (m^*) in the Γ - Y direction were estimated by parabolic-fitting at the band extrema (Fig. S14), and the extracted m^* s were 0.73, 0.44, and 0.52 for BTBT, BSBS, and BTeBTe, respectively. This strongly implies that the dimeric herringbone structure is not the detrimental factor for effective carrier transport.

Even with these two additional analyses on the solid-state properties, we could not find the rationale for the device

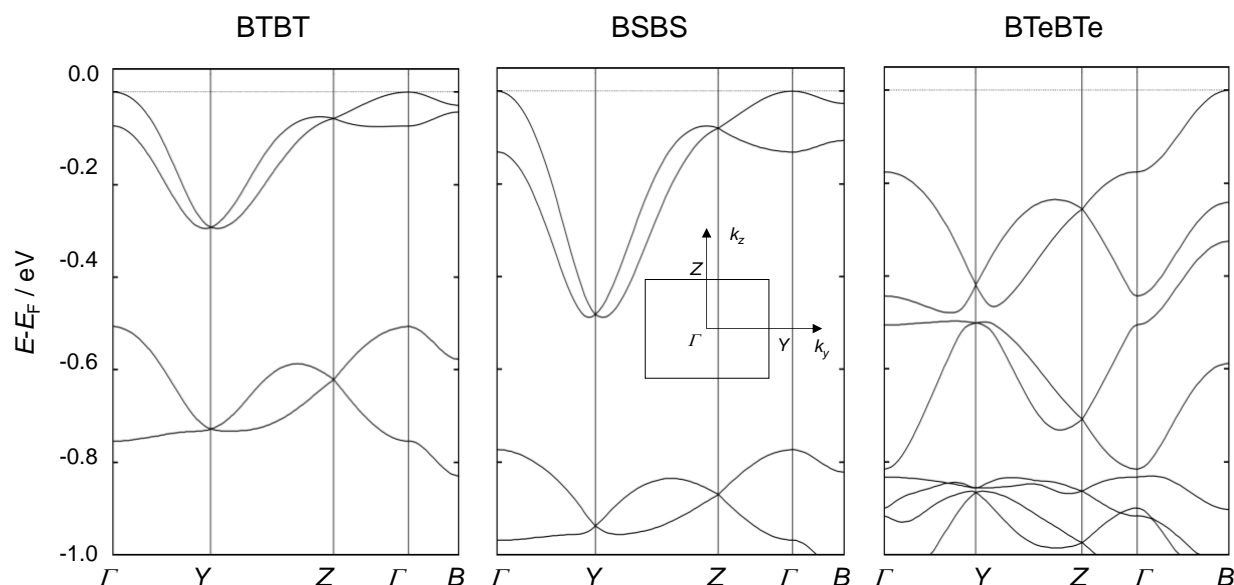


Fig. 8 The DFT-calculated band structures of BTBT, BSBS, and BTeBTe. The reciprocal coordinates of the high-symmetry points are: $\Gamma = (0\ 0\ 0)$, $Y = (0\ 1/2\ 0)$, $Z = (0\ 0\ 1/2)$, $B = (1/2\ 0\ 0)$. Note that only several valence bands just below the Fermi level are shown to clarify the differences between the band structures that closely relate to the hole transport. The inset represents the Brillouin zone diagram with respect to the crystallographic cell.

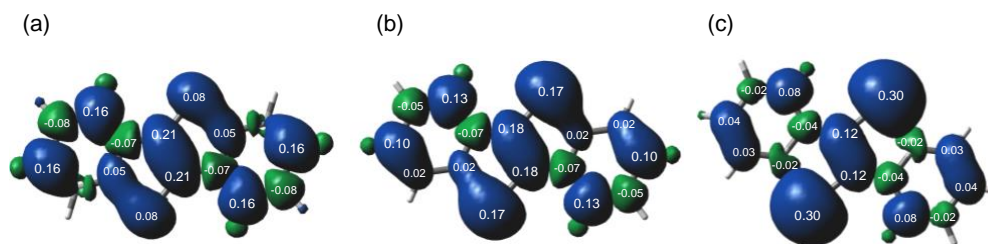


Fig. 9 Distribution of spin density in the radical cationic state of (a) BTBT, (b) BSBS and (c) BTeBTe. The numbers on the atoms are ratio of spins.

behaviour of BTeBTe. We thus turned our attention once again to molecular electronic structures. As already pointed out, BTeBTe has a distinct molecular electronic properties among the BXB system, which can be boiled down to the significant contribution of the tellurium atoms to the electronic structure of BTeBTe (Fig. 3). For the p-type organic semiconductors, the nature of HOMO is critically important, and in this regard, the fact that the HOMO coefficients strongly localized on the tellurium atoms could not be desirable for efficient carrier transport in the solid state, because the injected holes from the electrode tend to localize on the particular part of the molecules. In fact, the spin density calculated for the BTeBTe radical cation shows significant localization of spin on the tellurium atoms (Fig. 9c); approximately 60% spin density on the tellurium atoms. Furthermore, more than 80% spin density is localized on the central ditelluraethene (C_2Te_2) moiety, and the outermost benzene rings poorly contribute to spin delocalization. In sharp contrast, the spin density in BTBT- and BSBS- radical cations is delocalized over the π -framework (Fig. 9a and 9b). The localized spin on the tellurium atoms in BTeBTe tends to be less mobile in the solid state than the delocalized spin in BTBT and BSBS, implying that the nature of active carrier species in the working devices are affected by the chalcogen atoms in the molecular framework. Although we can not conclude that the strong localization nature of spin in the BTeBTe radical cation is the actual cause for the silent FET behaviour, the tellurium atoms in the BXB core could alter the nature of molecules in both the neutral and charged states, which can largely affect the mobility of active carrier in the crystal of BTeBTe.

Conclusions

The concept of “heavy-atom effects” have been regarded as an effective measure to improve the carrier mobility of organic semiconductors, since the carrier transport in organic semiconducting solid is governed by intermolecular orbital overlap, which can be enhanced by using “heavy” chalcogen atoms such as selenium and tellurium instead of sulphur atoms. With the BXB parent system, we have tried to verify the concept by elucidating the molecular electronic structures, packing structures and intermolecular interaction in the solid

state, the solid-state electronic structures, and carrier transport properties.

The substitution of the sulphur in BTBT with selenium atoms only slightly alters the molecular electronic properties and the packing structure, and thereby the electronic structure at the solid state are very similar to each other. As a result of the larger atomic radius and more diffused electron density of selenium than those of sulphur atoms, the intermolecular electronic couplings in BSBS are enhanced, which results in improved carrier mobility in the SC-OFETs of BSBS. This can be regarded as a positive side of “heavy-atom effect”. On the other hand, the substitution of the selenium in BSBS with tellurium atoms significantly changes not only the molecular electronic properties but also the packing structures. These significant changes can be explained by the nature of tellurium atom in the π -conjugated framework; poor conjugation in the π -system and low aromaticity of the tellurophene moiety, and the elongated C-Te bonds that distort a whole molecular structure. Consequently, the solid-state electronic structure of BTeBTe is significantly different from those of BTBT and BSBS. Furthermore it is somewhat surprising that the BTeBTe-based SC-OFETs show no transistor responses. Although we can not completely figure out the actual cause of the silent behaviours in the BTeBTe SC-OFETs, several distinctive features of BTeBTe as organic semiconductors, such as high-lying HOMO energy level, significant contribution of tellurium atoms to the molecular electronic structure both at the neutral and radical cation states, the dimeric herringbone structure with the relatively narrow HOMO band, are elucidated. These features may not be always positive in the application of BTeBTe to the FET channel. We believe, however, that to understand these distinctive features of tellurium-containing molecules could be useful in developing organic semiconductors in future.

Conflicts of interest

There are no conflicts to declare.

Acknowledgements

We thank Dr. Daisuke Hashizume in RIKEN for his help in solving the crystal structure of BTeBTe. We thank Dr. Lionel Hirsch, Marco Pereira in Univ. Bordeaux, IMS, CNRS for their assistance in the fabrication of SC-OFETs. We thank the Super-computer

System in the Advanced Center for Computing and Communication (ACCC) of RIKEN and the Center for Computational Materials Science, Institute for Materials Research, Tohoku University for the use of MASAMUNE-IMR (Materials science Supercomputing system for Advanced Multi-scale simulations towards Next-generation - Institute for Materials Research) for support in theoretical calculations. This work was financially supported by JSPS KAKENHI Grant Numbers JP15H02196 and JP19H00906, and the Bilateral Programs between Japan and France supported by JSPS and CNRS.

Notes and references

- C. Wang, H. Dong, W. Hu, Y. Liu and D. Zhu, *Chem. Rev.*, 2012, **112**, 2208-2267.
- H. Dong, X. Fu, J. Liu, Z. Wang and W. Hu, *Adv. Mater.*, 2013, **25**, 6158-6183.
- H. Sirringhaus, *Adv. Mater.*, 2014, **26**, 1319-1335.
- J. E. Anthony, *Chem. Rev.*, 2006, **106**, 5028-5048.
- K. Takimiya, S. Shinamura, I. Osaka and E. Miyazaki, *Adv. Mater.*, 2011, **23**, 4347-4370.
- K. Takimiya, I. Osaka, T. Mori and M. Nakano, *Acc. Chem. Res.*, 2014, **47**, 1493-1502.
- K. Takimiya, H. Ebata, K. Sakamoto, T. Izawa, T. Otsubo and Y. Kunugi, *J. Am. Chem. Soc.*, 2006, **128**, 12604-12605.
- H. Ebata, T. Izawa, E. Miyazaki, K. Takimiya, M. Ikeda, H. Kuwabara and T. Yui, *J. Am. Chem. Soc.*, 2007, **129**, 15732-15733.
- H. Iino, T. Usui and J.-i. Hanna, *Nat. Commun.*, 2015, **6**, 6828.
- H. Minemawari, M. Tanaka, S. Tsuzuki, S. Inoue, T. Yamada, R. Kumai, Y. Shimoi and T. Hasegawa, *Chem. Mater.*, 2017, **29**, 1245-1254.
- T. Yamamoto and K. Takimiya, *J. Am. Chem. Soc.*, 2007, **129**, 2224-2225.
- K. Niimi, S. Shinamura, I. Osaka, E. Miyazaki and K. Takimiya, *J. Am. Chem. Soc.*, 2011, **133**, 8732-8739.
- H. Minemawari, T. Yamada, H. Matsui, J. y. Tsutsumi, S. Haas, R. Chiba, R. Kumai and T. Hasegawa, *Nature*, 2011, **475**, 364-367.
- Y. Yuan, G. Giri, A. L. Ayzner, A. P. Zoombelt, S. C. B. Mannsfeld, J. Chen, D. Nordlund, M. F. Toney, J. Huang and Z. Bao, *Nat. Commun.*, 2014, **5**, 3005.
- During the preparation of this manuscript, single-crystal transistors of BTBT was reported; X. Liu, X. Su, C. Livache, L.-M. Chamoreau, S. Sanaur, L. Sosa-Vargas, J.-C. Ribierre, D. Kreher, E. Lhuillier, E. Lacaze and F. Mathevet, *Org. Electron.*, 2020, **78**, 105605.
- Y. Kunugi, K. Takimiya, K. Yamane, K. Yamashita, Y. Aso and T. Otsubo, *Chem. Mater.*, 2003, **15**, 6-7.
- A. Patra and M. Bendikov, *J. Mater. Chem.*, 2010, **20**, 422-433.
- A. A. Jahnke and D. S. Seferos, *Macromol. Rapid Commun.*, 2011, **32**, 943-951.
- E. I. Carrera and D. S. Seferos, *Macromolecules*, 2015, **48**, 297-308.
- K. Takimiya, Y. Kunugi, Y. Konda, H. Ebata, Y. Toyoshima and T. Otsubo, *J. Am. Chem. Soc.*, 2006, **128**, 3044-3050.
- T. Izawa, E. Miyazaki and K. Takimiya, *Chem. Mater.*, 2009, **21**, 903-912.
- H. Sugino and K. Takimiya, *Chem. Lett.*, 2017, **46**, 345-347.
- M. Saito, I. Osaka, E. Miyazaki, K. Takimiya, H. Kuwabara and M. Ikeda, *Tetrahedron Lett.*, 2011, **52**, 285-288.
- H. Sashida and S. Yasuike, *J. Heterocycl. Chem.*, 1998, **35**, 725-726.
- R. A. Laudise, C. Kloc, P. G. Simpkins and T. Siegrist, *J. Cryst. Growth*, 1998, **187**, 449-454.
- R. Zeis, T. Siegrist and C. Kloc, *Appl. Phys. Lett.*, 2005, **86**, 022103.
- Gaussian 16, Revision C.01, M. J. Frisch, G. W. Trucks, H. B. Schlegel, G. E. Scuseria, M. A. Robb, J. R. Cheeseman, G. Scalmani, V. Barone, G. A. Petersson, H. Nakatsuji, X. Li, M. Caricato, A. V. Marenich, J. Bloino, B. G. Janesko, R. Gomperts, B. Mennucci, H. P. Hratchian, J. V. Ortiz, A. F. Izmaylov, J. L. Sonnenberg, Williams, F. Ding, F. Lipparini, F. Egidi, J. Goings, B. Peng, A. Petrone, T. Henderson, D. Ranasinghe, V. G. Zakrzewski, J. Gao, N. Rega, G. Zheng, W. Liang, M. Hada, M. Ehara, K. Toyota, R. Fukuda, J. Hasegawa, M. Ishida, T. Nakajima, Y. Honda, O. Kitao, H. Nakai, T. Vreven, K. Throssell, J. A. Montgomery Jr., J. E. Peralta, F. Ogliaro, M. J. Bearpark, J. J. Heyd, E. N. Brothers, K. N. Kudin, V. N. Staroverov, T. A. Keith, R. Kobayashi, J. Normand, K. Raghavachari, A. P. Rendell, J. C. Burant, S. S. Iyengar, J. Tomasi, M. Cossi, J. M. Millam, M. Klene, C. Adamo, R. Cammi, J. W. Ochterski, R. L. Martin, K. Morokuma, O. Farkas, J. B. Foresman and D. J. Fox, Gaussian, Inc., Wallingford CT, 2016.
- G. R. Hutchison, M. A. Ratner and T. J. Marks, *J. Am. Chem. Soc.*, 2005, **127**, 2339-2350.
- ADF: powerful DFT code for modeling molecules; Scientific Computing and Modeling: Amsterdam; <http://www.scm.com/ADF/>.
- A. Troisi and G. Orlandi, *Phys. Rev. Lett.*, 2006, **96**, 086601.
- S.-H. Wen, A. Li, J. Song, W.-Q. Deng, K.-L. Han and W. A. Goddard, *J. Phys. Chem. B*, 2009, **113**, 8813-8819.
- J. J. McKinnon, M. A. Spackman and A. S. Mitchell, *Acta Crystallogr. Sect. B*, 2004, **60**, 627-668.
- M. J. Turner, J. J. McKinnon, S. K. Wolff, D. J. Grimwood, M. A. Spackman, D. Jayatilaka and M. A. Spackman, CrystalExplorer17 (2017). University of Western Australia. <http://hirshfeldsurface.net>.
- B. Jeziorski, R. Moszynski and K. Szalewicz, *Chem. Rev.*, 1994, **94**, 1887-1930.
- R. M. Parrish, L. A. Burns, D. G. A. Smith, A. C. Simmonett, A. E. DePrince, E. G. Hohenstein, U. Bozkaya, A. Y. Sokolov, R. Di Remigio, R. M. Richard, J. F. Gonthier, A. M. James, H. R. McAlexander, A. Kumar, M. Saitow, X. Wang, B. P. Pritchard, P. Verma, H. F. Schaefer, K. Patkowski, R. A. King, E. F. Valeev, F. A. Evangelista, J. M. Turney, T. D. Crawford and C. D. Sherrill, *J. Chem. Theory Comput.*, 2017, **13**, 3185-3197.
- R. Dovesi, A. Erba, R. Orlando, C. M. Zicovich-Wilson, B. Civalleri, L. Maschio, M. Rérat, S. Casassa, J. Baima, S. Salustro and B. Kirtman, *WIREs Comput. Mol. Sci.*, 2018, **8**, e1360.
- M. Z. S. Flores, V. N. Freire, R. P. dos Santos, G. A. Farias, E. W. S. Caetano, M. C. F. de Oliveira, J. R. L. Fernandez, L. M. R. Scolfaro, M. J. B. Bezerra, T. M. Oliveira, G. A. Bezerra, B. S. Cavada and H. W. Leite Alves, *Physical Review B*, 2008, **77**, 115104.
- E. Vessally, *J. Struct. Chem.*, 2008, **49**, 979-985.

39. C. Niebel, Y. Kim, C. Ruzié, J. Karpinska, B. Chattopadhyay, G. Schweicher, A. Richard, V. Lemaire, Y. Olivier, J. Cornil, A. R. Kennedy, Y. Diao, W.-Y. Lee, S. Mannsfeld, Z. Bao and Y. H. Geerts, *J. Mater. Chem. C*, 2015, **3**, 674-685.
40. K. Takimiya, Y. Konda, H. Ebata, N. Niihara and T. Otsubo, *J. Org. Chem.*, 2005, **70**, 10569-10571.
41. G. Gryn'ova and C. Corminboeuf, *J. Phys. Chem. Lett.*, 2016, **7**, 5198-5204.
42. G. R. Desiraju and A. Gavezzotti, *Acta Crystallogr. Sect. B*, 1989, **45**, 473-482.
43. F. P. A. Fabbiani, D. R. Allan, S. Parsons and C. R. Pulham, *Acta Crystallogr. Sect. B*, 2006, **62**, 826-842.
44. M. Matsumura, A. Muranaka, R. Kurihara, M. Kanai, K. Yoshida, N. Kakusawa, D. Hashizume, M. Uchiyama and S. Yasuike, *Tetrahedron*, 2016, **72**, 8085-8090.
45. M. Hultell and S. Stafström, *Chem. Phys. Lett.*, 2006, **428**, 446-450.
46. T. Yamamoto, S. Shinamura, E. Miyazaki and K. Takimiya, *Bull. Chem. Soc. Jpn.*, 2010, **83**, 120-130.